 

PACS numbers: 42.30.Wb; 87.57.cm; 87.63.L – ; 87.64.Cc
DOI: 10.1070/QE2008v038n06ABEH013839

# Shadow noise in OCT images of biological tissues

L.S. Dolin, E.A. Sergeeva, I.V. Turchin

***Abstract*. Optical coherence tomography (OCT) images of turbid medium with spatially fluctuating optical parameters demonstrate the presence of spatial noise ('shadow noise') caused by shading of the observed layer by variations in scattering and absorption coefficients of superficial layers. In this paper we report the development of the theoretical model of shadow noise in OCT images in which the features for discriminating this type of noise from the noise of a different origin are determined. Shadow noise is discovered in OCT images of biological tissue after specific image processing and the validity of the developed theoretical model is proven. The role of shadow noise as an interfering factor at imaging the variations in the backscattering coefficient, as well as the source of extra information on optical characteristics of the medium is analysed.**

***Keywords***: *optical coherence tomography, random scattering medium, statistical OCT image analysis.*

## 1. Introduction

Analytical models of optical coherence tomography (OCT) of biological tissues [1 – 3] are mainly based on the theory of radiation transfer in media with uniform or regularly variable optical properties. It is commonly assumed that the stochastic behaviour of an OCT signal is caused by speckle noise [4 – 5] or instrumental noise of different origins. However, the irregularity of the OCT signal can also be the result of random spatial variations in optical parameters of the observed medium.

OCT images or laser pulsed tomography images of statistically random turbid media typically allow for visualisation of the variations in the backscattering coefficient. At the same time, they demonstrate the effects of a probing beam decay along the propagation path. Even in the simplest case of a plane-layered turbid medium, the OCT image of such a structure with stratified backscattering would be obscured due to absorption and small-angle scattering of the probing beam. In the case of three-dimensional variations in optical characteristics, the probing beam extinction depends not only on the imaging depth but also on the relative lateral position of the OCT probe end. In such a medium the image of the observed layer is blurred by the so-called 'spatial noise' since the imaging plane is illuminated by light which is inhomogeneously transmitted by upper layers. Localised reflecting inclusions can in the same way cause inhomogeneous shading of the underlying plane as long as they cause nonuniform transmission of the probing beam. In theoretical models of light propagation in turbid media with a high degree of scattering anisotropy, the large-angle scattering is often considered as additional dissipation described by the effective absorption coefficient so that the total absorption is approximately equal to a sum of the true absorption coefficient and doubled backscattering coefficient. Therefore, shadow noise in OCT images of the medium with random variations in backscattering can be, to a first approximation, described by the analytical model developed for media with a spatially fluctuating absorption coefficient.

Pioneer studies of light propagation in media with random optical scattering and absorption were related to the problem of the Earth radiation regime [6]. Primitive theoretical models considered the plane-layered geometry of scattering objects with a fluctuating optical thickness or with smooth variations in optical parameters. Later, the statistical models of radiation transport in turbid media with 3D variations in scattering and absorption were developed [7 – 11]. It was demonstrated that variations in optical parameters result in a decrease in the attenuation coefficient of a statistically average radiation field (the 'sieve effect'). The sieve effect affects the results of estimates of the absorber concentration in the medium evaluated from measurements of optical transmittance [9, 10] or intrinsic thermal radiation measurements [11]. Different approaches were developed to analyse high-order statistical characteristics of the radiation field [8, 12]. For the case of a laser beam propagating in a turbid medium with spatially fluctuating absorption and scattering and a narrow scattering phase function, the equations for the average radiance and radiance spatial correlation function were derived [8]. The obtained equations allowed one to quantitatively characterise the effect of the random radiance modulation in a narrow optical beam upon its multiple passage through the absorbing inhomogeneities, as well as the smoothing effect of radiance fluctuations caused by multiple forward scattering [8, 13, 14]. The problem of visualisation of a self-illuminating object embedded into a turbid medium with fluctuating optical properties was also investigated [15, 16].

**L.S. Dolin, E.A. Sergeeva, I.V. Turchin** Institute of Applied Physics, Russian Academy of Science, ul. Ul'yanova 46, 603950 Nizhny Novgorod, Russia; e-mail: sea@ufp.appl.sci-nnov.ru

Received 30 January 2008; revision received 13 March 2008
*Kvantovaya Elektronika* **38** (6) 543 – 550 (2008)
Translated by L.S. Dolin

In the present paper the influence of statistical variations in optical properties on OCT images of the turbid medium is studied. The theory of shadow noise is developed and the analysis of shadow noise statistical characteristics is performed. Finally, the experimental data, which reveal the presence of shadow noise in OCT images of biological tissues, are demonstrated.

## 2. Theory of shadow noise

### 2.1 Formulation of the problem

Consider a semi-infinite slab of a turbid medium with highly anisotropic scattering described by the scattering phase function $p_0(\theta)$ as the function of the scattering angle $\theta$, and spatially inhomogeneous distribution of the absorption coefficient $\mu_a(\boldsymbol{r})$ and backscattering coefficient $\mu_{bs}(\boldsymbol{r})$. The vector $\boldsymbol{r}$ defines the 3D position of the observation point with respect to the point of origin. The probing beam of the OCT setup enters the medium parallel to the $z$ axis which is directed in-depth. We quantify random optical parameters of the medium by mean values of the absorption coefficient $\langle\mu_a\rangle$ and the backscattering coefficient $\langle\mu_{bs}\rangle$ assuming them to be statistically uniform, and deviations, $\tilde{\mu}_a(\boldsymbol{r})=\mu_a(\boldsymbol{r})-\langle\mu_a\rangle$, $\tilde{\mu}_{bs}(\boldsymbol{r})=\mu_{bs}(\boldsymbol{r})-\langle\mu_{bs}\rangle$ with zero means. The scattering phase function $p_0(\theta)$ can be presented as the sum of a forward-peaked function $p_1(\theta)$ and an isotropic component. The first term is characterised by the variance $\langle\theta^2\rangle$:

$$\langle\theta^2\rangle=\int_0^\pi\theta^2 p_1(\theta)\sin\theta\,\mathrm{d}\theta\Big/\int_0^\pi p_1(\theta)\sin\theta\,\mathrm{d}\theta. \tag{1}$$

The scattering coefficient $\mu_s(\boldsymbol{r})$ can also be split into two components, i.e. the coefficient of small-angle scattering, or forward scattering, $\mu_{fs}$, and the coefficient of isotropic scattering equal to the doubled backscattering coefficient [17]:

$$\mu_s(\boldsymbol{r})=\mu_{fs}+2\mu_{bs}(\boldsymbol{r}).$$

Hereafter we consider propagation of the probing beam in the effective medium with small-angle scattering parameters $\mu_{fs}$ and $p_1(\theta)$, and with the effective absorption coefficient $\mu_a^{\mathrm{eff}}(\boldsymbol{r})=\mu_a(\boldsymbol{r})+2\mu_{bs}(\boldsymbol{r})$ which accounts for energy losses due to absorption and large-angle scattering. Note that the total extinction coefficient of the considered effective medium, $\mu_t=\mu_a^{\mathrm{eff}}(\boldsymbol{r})+\mu_{fs}$, is equal to that of the original medium. The random term of the attenuation coefficient, $\tilde{\mu}_t=\mu_t-\langle\mu_t\rangle$, corresponds to the random component of the effective absorption coefficient $\tilde{\mu}_a^{\mathrm{eff}}=\tilde{\mu}_a+2\tilde{\mu}_{bs}$. Fluctuations of optical parameters are described by corresponding autocorrelation functions:

$$B_t(\boldsymbol{\rho})=\langle\tilde{\mu}_t(\boldsymbol{r}+\boldsymbol{\rho})\tilde{\mu}_t(\boldsymbol{r})\rangle,\quad B_s(\boldsymbol{\rho})=\langle\tilde{\mu}_{bs}(\boldsymbol{r}+\boldsymbol{\rho})\tilde{\mu}_{bs}(\boldsymbol{r})\rangle. \tag{2}$$

The OCT image of a random medium is formed by measuring the backscattered power $P(\boldsymbol{r}_\perp,z)$ as the function of the transverse position of the probing-beam end with respect to the origin $\boldsymbol{r}_\perp$, and the imaging depth $z$. The value of the OCT signal from the depth $z$ in the turbid medium is defined by the intensity $I(\boldsymbol{r}_\perp,\boldsymbol{r}'_\perp,z)$ in the imaging plane $z=\mathrm{const}$ and obeys the relation [18]

$$P(\boldsymbol{r}_\perp,z)=K\iint_\infty[\langle\mu_{bs}(z)\rangle+\tilde{\mu}_{bs}(\boldsymbol{r}'_\perp,z)]I^2(\boldsymbol{r}_\perp,\boldsymbol{r}'_\perp,z)\mathrm{d}\boldsymbol{r}'_\perp, \tag{3}$$

where the factor $K$ accounts for the detector properties and does not influence the image structure. As follows from (3), the transverse variation in the OCT signal from the depth $z$ is caused either by backscattering coefficient variations in the imaging plane or by intensity fluctuations, which are accumulated as the beam propagates through upper layers. The values of $\mu_{bs}$ and $I^2$ in (3) are statistically independent, therefore, the average OCT signal is expressed via the average backscattering coefficient and the mean value of the squared intensity:

$$\langle P(\boldsymbol{r}_\perp,z)\rangle=K\langle\mu_{bs}(z)\rangle\iint_\infty\langle I^2(\boldsymbol{r}_\perp,\boldsymbol{r}'_\perp,z)\rangle\mathrm{d}\boldsymbol{r}'_\perp. \tag{4}$$

Shadow noise caused by intensity fluctuations in the probing beam can be characterised by statistical variations in the first term in (3):

$$P_1(\boldsymbol{r}_\perp,z)=K\langle\mu_{bs}(z)\rangle\iint_\infty I^2(\boldsymbol{r}_\perp,\boldsymbol{r}'_\perp,z)\mathrm{d}\boldsymbol{r}'_\perp. \tag{5}$$

The second term of expression (3)

$$P_2(\boldsymbol{r}_\perp,z)=K\iint_\infty\tilde{\mu}_{bs}(\boldsymbol{r}'_\perp,z)I^2(\boldsymbol{r}_\perp,\boldsymbol{r}'_\perp,z)\mathrm{d}\boldsymbol{r}'_\perp \tag{6}$$

allows one to evaluate OCT signal deviations related to variations in the backscattering coefficient.

### 2.2 Shadow noise in the OCT signal formed by ballistic photons

The simplest model of shadow noise in the OCT signal is based on the assumption that the OCT image of the medium is formed mainly by ballistic photons which pass through the medium along straight trajectories. The intensity of the ballistic component in the medium with random absorption is given by the expressions

$$I(\boldsymbol{r}_\perp,\boldsymbol{r}'_\perp,z)=F(\boldsymbol{r}'_\perp-\boldsymbol{r}_\perp)\exp(-\langle\mu_t\rangle z-\varphi), \tag{7}$$

$$\varphi=\int_0^z\tilde{\mu}_t(\boldsymbol{r}'_\perp,z')\mathrm{d}z'.$$

Here $F(\boldsymbol{r}_\perp)$ is the intensity distribution in the collimated probing beam at the boundary of the medium. If the imaging depth $z$ is large with respect to the correlation length of the total attenuation coefficient fluctuations then the distribution of $\varphi$ obeys normal statistics even for non-Gaussian statistics for the $\tilde{\mu}_t$ function. Using the relation [19]

$$\langle\exp(-\varphi)\rangle=\exp\left(\langle\varphi^2\rangle/2\right), \tag{8}$$

the average OCT signal and its spatial correlation function can be evaluated from (4), (5) and (7):

$$\langle P(z)\rangle=K\langle\mu_{bs}\rangle\exp[-(2\mu_{\mathrm{eff}}-A_0)z]\iint_\infty F^2(\boldsymbol{r}_\perp)\mathrm{d}\boldsymbol{r}_\perp, \tag{9}$$

$$\Gamma(\boldsymbol{\rho}_\perp,z)=\langle P(\boldsymbol{r}_\perp+\boldsymbol{\rho}_\perp/2,z)P(\boldsymbol{r}_\perp-\boldsymbol{\rho}_\perp/2,z)\rangle=K^2\langle\mu_{bs}\rangle^2\times$$

$$\times \exp[-2z(2\mu_{\text{eff}} - A_0)] \iint_{\infty} F^2(\boldsymbol{r}'_\perp - \boldsymbol{r}_\perp - \boldsymbol{\rho}_\perp/2, z)$$

$$\times F^2(\boldsymbol{r}''_\perp - \boldsymbol{r}_\perp + \boldsymbol{\rho}_\perp/2, z) \exp[4A(\boldsymbol{r}'_\perp - \boldsymbol{r}''_\perp)] \mathrm{d}\boldsymbol{r}'_\perp \mathrm{d}\boldsymbol{r}''_\perp. \quad (10)$$

Expressions (9) and (10) refer to the two-dimensional autocorrelation function of total attenuation fluctuations

$$A(\boldsymbol{\rho}_\perp) = \int_{-\infty}^{\infty} B_{\text{t}}(\boldsymbol{\rho}_\perp, \rho_z) \mathrm{d}\rho_z, \quad (11)$$

where $A_0 = A(0)$ is the variance of $\tilde{\mu}_{\text{t}}$ transverse fluctuations. The parameter $\mu_{\text{eff}} = \langle \mu_{\text{t}} \rangle - A_0/2$ is the effective attenuation coefficient in the medium with spatially fluctuating optical properties [8]. Further analysis is performed for Gaussian-shaped distributions of $F(\boldsymbol{r}_\perp)$ and $A(\boldsymbol{\rho}_\perp)$ with the transversal scale $r_0$ and the fluctuation correlation length $a$, correspondingly:

$$A(\boldsymbol{\rho}_\perp) = A_0 \exp\left(-\frac{\rho_\perp^2}{a^2}\right), \quad F(\boldsymbol{r}_\perp) = \exp\left(-\frac{\boldsymbol{r}_\perp^2}{r_0^2}\right). \quad (12)$$

To evaluate the integration in the right-hand part of (10) the following asymptotic relation is used:

$$\exp[C\exp(-x^2)] \approx (\exp C - 1)\exp\left[(-x^2(1 + C^2)^{1/2}\right].$$

The resulting expressions for the average OCT signal and the correlation function of OCT signal relative fluctuations are thus calculated from (9), (10) and allow for clear physical interpretation:

$$\langle P(z) \rangle = \frac{\pi r_0^2}{2} K \langle \mu_{\text{bs}} \rangle \exp(-2\langle \mu_{\text{t}} \rangle z + 2\zeta), \quad (13)$$

$$\gamma(\rho_\perp) = \frac{\Gamma(\rho_\perp)}{\langle P(z) \rangle^2} - 1$$

$$= \frac{\exp(4\zeta) - 1}{1 + (r_0/a)^2\left[1 + (4\zeta)^2\right]^{1/2}} \exp\left(-\frac{\rho_\perp^2}{\rho_{\text{c}}^2}\right). \quad (14)$$

In the latter expressions the dimensionless probing depth $\zeta$ and the correlation length of OCT signal relative fluctuations $\rho_{\text{c}}$ are introduced:

$$\zeta = A_0 z, \quad \rho_{\text{c}} = \left\{r_0^2 + a^2\left[1 + (4A_0 z)^2\right]^{-0.5}\right\}^{1/2}. \quad (15)$$

The variance of OCT signal relative fluctuations can be obtained from (14) as $\delta^2 = \gamma(0)$.

Expression (13) demonstrates the above mentioned 'sieve effect', a phenomenon of optical clearing of the turbid medium due to the random spatial distribution of absorbers [10]. As follows from (13), the sieve effect efficiency in the average OCT signal from the depth $z$ is higher than that in the intensity distribution at the doubled imaging depth $2z$. It is shown in [13] that the ratio of transmission coefficients for an inhomogeneous versus homogeneous turbid layer with the thickness of $2z$ is equal to $\exp\zeta$, while expression (13) contains the factor of $\exp(2\zeta)$. This means that the average transparency of the medium with fluctuating absorption or backscattering is different for the transmission mode and for the reflection mode. Increased optical clearing in the reflection mode is caused by a double passage of light through the same inhomogeneities of the absorption coefficient. The effect of the double passage is also the reason of the enhanced fluctuations in the OCT signal from the depth $z$ compared to the radiance fluctuations at the depth $2z$. It is clear from (14) that at small depths the variance of OCT signal fluctuations is linearly proportional to the imaging depth ($\delta^2 \approx 4\zeta$), whereas the variance of radiance fluctuations obeys the dependence $\delta^2 \approx \zeta$ [13]. Therefore the variance of radiance fluctuations at the depth $2z$ is twice low compared to that in the OCT signal from the depth $z$. This result is related to the effect of phase fluctuation doubling in the radar signal upon its back-and-forth passage through the same inhomogeneities of the refractive index [20].

The value of $A_0$ is proportional to the magnitude of the variance of attenuation coefficient fluctuations ($\langle \tilde{\mu}_{\text{t}}^2 \rangle$) and to its longitudinal correlation length. For isotropic fluctuations characterised by a Gaussian-shaped correlation function with the correlation scale $a$, one obtains $A_0 = \sqrt{\pi}\langle \tilde{\mu}_{\text{t}}^2 \rangle a$. Therefore, the parameter $\zeta$ is related to the dimensionless size of a single inhomogeneity, $\tau_a = \langle \tilde{\mu}_{\text{t}}^2 \rangle^{1/2} a$, and the number of inhomogeneities along the probe beam path, $N = z/a$, as

$$\zeta \approx \tau_{\text{a}} N.$$

The variance of OCT signal relative fluctuations as the function of the imaging depth is shown in Fig. 1a. According to (14), the variance does not depend on the average characteristics of the medium. As the imaging depth grows, the variance of OCT signal fluctuations increases, while the transversal correlation length $\rho_{\text{c}}$ decreases (Fig. 1b). This effect is caused by broadening of the fluctuation spectrum as the probing beam propagates through the medium with the inhomogeneous transparency.

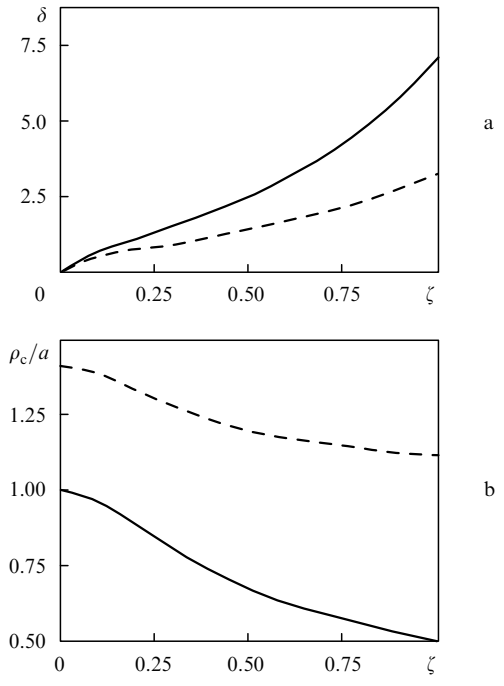


**Figure 1.** Variance of OCT signal relative fluctuations (a), and its correlation length related to the size of a single inhomogeneity (b) as the function of the imaging depth $\zeta$ for $r_0/a = 0.1$ (solid curves) and $r_0/a = 1$ (dashed curves).

### 2.3 Shadow noise in the OCT image formed by multiply scattered light

The model of shadow noise in the OCT signal described above is valid for small imaging depths where the contribution of multiple scattering to the OCT signal is negligible. The ballistic regime in the OCT image is limited by the depth $z_0$ which can be estimated from the equation

$$(\mu_{\rm fs} z_0)^3 \exp(-\mu_{\rm fs} z_0) = B$$

with the dimensionless parameter $B$. The latter shows the relation between the probing beam radius and the transverse divergence of a scattered photon at a single free path:

$$B = \frac{3(\mu_{\rm fs} r_0)^2}{\langle \theta^2 \rangle}, \tag{16}$$

At depths $z > z_0$ the probing beam blurs due to multiple small-angle scattering and the OCT signal is formed by backscattering of the broadened beam. At the same time, in the presence of multiple scattering, spatial variations in the probing beam intensity caused by inhomogeneous absorption are smoothened out and the increase in fluctuations is restrained. It was demonstrated [20] that the effect of scattering on the intensity fluctuations depends on the dimensionless parameter

$$Q = \left( \frac{2A_0^3 a^2}{\mu_{\rm fs} \langle \theta^2 \rangle} \right)^{1/4}. \tag{17}$$

In the case of $Q < 2$, intensity fluctuations in the probing beam decay as the imaging depth grows. The variance of the probing intensity relative fluctuation tends to a limit value proportional to the parameter $Q$. For the values $Q > 2$, the variance of intensity fluctuations increases exponentially with the depth.

As follows from (5), the second statistical moment of the OCT signal is expressed via the fourth moment of the probing intensity. Due to the lack of an accurate analytical model of $\langle I^4 \rangle$ accounting for multiple scattering the statistical moments of the OCT signal are derived by assuming that the probing intensity fluctuations are small. Further evaluation is performed using the existing model of the spatial correlation function of intensity relative fluctuations $\delta I = I/\langle I \rangle - 1$ in a narrow probing beam at depths $z \gg z_0$ [13]:

$$\gamma_I(\boldsymbol{\rho}_\perp, z) = \langle \delta I(\boldsymbol{r}_\perp + \boldsymbol{\rho}_\perp/2, z) \delta I(\boldsymbol{r}_\perp - \boldsymbol{\rho}_\perp/2, z) \rangle.$$

The variance of OCT signal relative fluctuations is then expressed via the average intensity distribution in the imaging plane, $\bar{I}(\boldsymbol{r}'_\perp, z) = \langle I(\boldsymbol{r}_\perp, \boldsymbol{r}_\perp + \boldsymbol{r}'_\perp, z) \rangle$, as

$$\delta^2(z) = \frac{\langle P^2(z) \rangle}{\langle P(z) \rangle^2} - 1 = \frac{4 \iint_\infty \iint_\infty \bar{I}^2(\boldsymbol{r}'_\perp, z) \bar{I}^2(\boldsymbol{r}''_\perp, z) \gamma_I(|\boldsymbol{r}'_\perp - \boldsymbol{r}''_\perp|, z) {\rm d}\boldsymbol{r}'_\perp {\rm d}\boldsymbol{r}''_\perp}{\left[ \iint_\infty \bar{I}^2(\boldsymbol{r}'_\perp, z) {\rm d}\boldsymbol{r}'_\perp \right]^2}. \tag{18}$$

The average intensity in the multiply scattering medium can be calculated from the equation of radiative transfer in the small-angle diffusion approximation:

$$\bar{I}(\boldsymbol{r}_\perp, z) = \frac{\exp(-\langle \mu_{\rm a} \rangle z - r_\perp^2/S_{\rm s})}{\pi S_{\rm s}}, \tag{19}$$

$$S_{\rm s} = r_0^2 \left( 1 + \frac{\tau_{\rm s}^3}{B} \right), \quad \tau_{\rm s} = \mu_{\rm fs} z. \tag{20}$$

To perform integration in (18) the correlation function of intensity relative fluctuations is assumed to be Gaussian:

$$\gamma_I(\rho_\perp, z) = \delta_I^2 \exp\left( -\frac{\rho_\perp^2}{\rho_I^2} \right). \tag{21}$$

As a result, the variance of OCT signal relative fluctuations expressed via the variance of the probing intensity fluctuations $\delta_I^2$, its transverse correlation length $\rho_I$, and the probing beam cross section $S_{\rm s}$ at the depth $z$ inside scattering medium has the form:

$$\delta^2 = \frac{4\delta_I^2}{1 + S_{\rm s}/\rho_I^2}. \tag{22}$$

For the following numerical analysis we use integral expressions for $\delta_I^2$ and $\rho_I$ in accordance with [13]. The dependence of $\delta^2(\zeta)$ on the imaging depth $\zeta$ is defined by dimensionless parameters $Q$ and $B$ from (16) and (17), respectively, and by the ratio of the incident beam radius to the correlation scale of absorption fluctuations $r_0/a$ [see Eqn (12)].

At small imaging depths ($\zeta \to 0$) the variance of OCT signal fluctuations is described by the same asymptotic expression both for ballistic and multiple small-angle scattering regimes:

$$\delta^2 \approx 4\zeta [1 + (r_0/a)^2]^{-1}.$$

However, this approximation is valid within a limited range of $\zeta$, which is getting smaller as the magnitude of $Q$ decreases. Figure 2 demonstrates that in the case of strong scattering the variance of OCT signal fluctuation grows up to the depth $\zeta_{\rm m}$ and then decreases. The depth $\zeta_{\rm m}$ of maximum fluctuations depends on the value of $Q$ ($\zeta_{\rm m} \approx Q$ in the range $Q < 0.5 - 0.6$).

### 2.4 Two-term analytical model of shadow noise in the OCT signal

The model of shadow noise formed by multiply scattered light provides, in general, a correct description of the OCT signal fluctuation dependence on the imaging depth. However quantitative values of the fluctuation variance are underestimated in the vicinity of $\zeta_{\rm m}$ since this model does not take into account the contribution of ballistic photons to the backscattered signal. Therefore, we propose the advanced approach by combining the two previously discussed models into a two-term hybrid model which considers both the effect of ballistic photons and the contribution of multiply scattered photons to shadow noise. According to the hybrid model, the total intensity in the probing beam is split into two components, one is formed by ballistic photons and the other is produced by multiply scattered light. The variance of the relative intensity fluctuation is thus represented as a sum of variances of individual intensity components weighted by the factors proportional to the energy of each component. Within the framework of the hybrid model, the variance of OCT signal

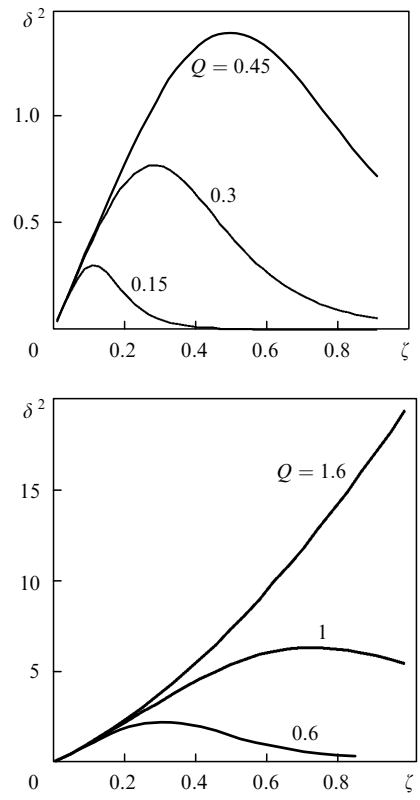


**Figure 2.** Variance $\delta^2$ of OCT signal relative fluctuations as a function of the imaging depth $\zeta$ for $B = 0.1$, $r_0/a = 0.1$ and various values of $Q$.

relative fluctuations is expressed via partial variances $\delta_1$ and $\delta_2$, which are calculated from (14) and (22), respectively:

$$\delta^2 = \alpha^2\delta_1^2 + 2\alpha(1-\alpha)\delta_1\delta_2 + (1-\alpha)^2\delta_2^2, \tag{23}$$

$$\alpha = [1 + 4(1+\beta)^{-1}(\exp\tau_s - 1) + \beta^{-1}(\exp\tau_s - 1)^2]^{-1}, \tag{24}$$

$$\beta = 1 + B^{-1}\tau_s^3[1 - \exp(-\tau_s)]^{-1}, \tag{25}$$

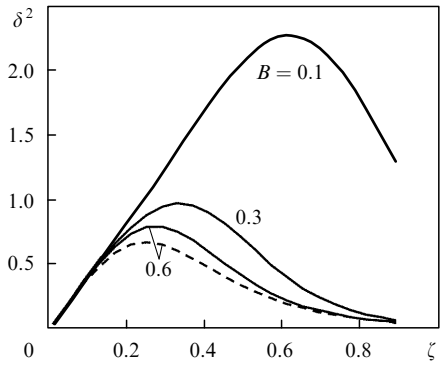


**Figure 3.** Variance of OCT signal relative fluctuations versus the imaging depth for the values $Q = 0.3$, $r_0/a = 0.3$ and various values of $B$. The curves are plotted for the model which takes into account multiple scattering (dashed curve) and the two-term hybrid model (solid curve).

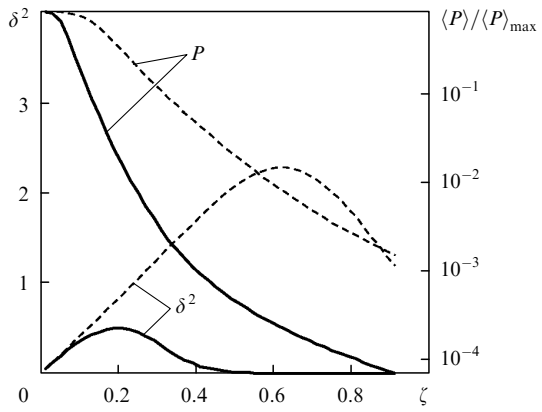


**Figure 4.** Average OCT signal related to its maximum value $\langle P\rangle/\langle P\rangle_{max}$ and the variance of OCT signal relative fluctuations as a function of the imaging depth for the values $B = 0.1$, $r_0/a = 0.3$, $Q = 0.15$ (solid curves), $Q = 0.3$ (dashed curves).

The discrepancy in the values of the variance calculated from (22) and (23) strictly depends on the parameter $B$. Figure 3 demonstrates that this discrepancy decreases with increasing $B$ (which can be done by increasing the incident beam dimensionless radius $\mu_{fs}r_0$ or by decreasing the scattering angle variance). On the contrary, for an optically thin probing beam, a significant difference in the values of the variance calculated from (22) and from (23) is observed.

Figure 4 shows the dependence of the variance of OCT signal fluctuations together with the profile of the average OCT signal on the imaging depth. The highest level of fluctuations is observed at the depths where OCT signal is decreased for less than 20 dB.

Figures 5 and 6 demonstrate the influence of absorber distribution characteristics ($A_0/\mu_{fs}$ and $\mu_{fs}a$) on the variance of the signal fluctuations from the imaging depth $\tau_s = \mu_{fs}z$. One can see from Fig. 5 that when the absorber size (related to the scattering free path) increases, the maximum fluctuation level and the value of $\zeta_m$ grow. As the variance of absorption fluctuations ($A_0$) increases, the level of maximum OCT signal fluctuations raises without shifting its longitudinal position.

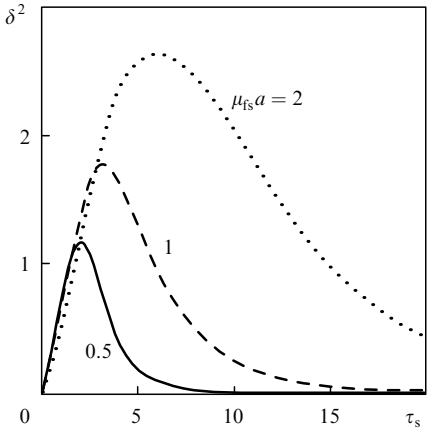


**Figure 5.** Dependences of the fluctuation variance $\delta^2(\tau_s)$ on the depth for the values $A_0/\mu_{fs} = 0.15$, $\langle\theta^2\rangle = 0.08$, $\mu_{fs}r_0 = 0.1$ and various values of $\mu_{fs}a$.

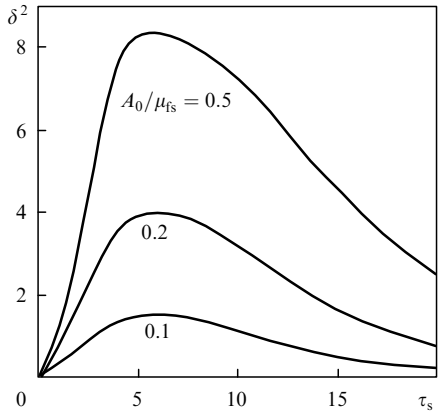


**Figure 6.** The $\delta^2(\tau_s)$ dependence for the values $\langle\theta^2\rangle = 0.08$, $\mu_{fs}r_0 = 0.1$, $\mu_{fs}a = 0.2$ and various values of $A_0/\mu_{fs}$.

## 3. Experimental study of shadow noise in OCT images

Experimental study of shadow noise in OCT images of phantom samples has been performed by using the OCT device developed at the Institute of Applied Physics, RAS [3]. The output power of the device is 0.75 mW at the working wavelength 1.3 μm. The system provides 15-μm spatial resolution both in transverse and axial directions and operates at a rate of 100 A-scans per second. Along with phantom samples, a set of clinical OCT images of mucous biological tissues have been analysed to reveal the presence of shadow noise. In the processing algorithm, the variance of OCT signal relative fluctuations is calculated over each transverse line of a 2D image corresponding to a definite imaging depth. The dependence of the fluctuation variance is then plotted as a function of the depth.

Figure 7 shows the OCT image of a scattering phantom with a random distribution of absorption and the result of its processing. The phantom is a 25 % aqueous solution of Intralipid 10 % with a bundle of hair embedded. The OCT image displays evolution of the shadow structure with a gradual developing of transversal fluctuations. Figure 7 (bottom) demonstrates the result of OCT image processing. Average optical characteristics of the phantom sample, i.e. scattering coefficient $\mu_{fs}$ and the parameter $\langle\theta^2\rangle$ of scattering phase function, have been obtained from the OCT signal dependence versus the depth on the basis of the numerical algorithm described in [21]. The statistical characteristics of the inhomogeneous absorption distribution are evaluated by fitting the experimental dependence $\delta^2(z)$ with that obtained from the theory.

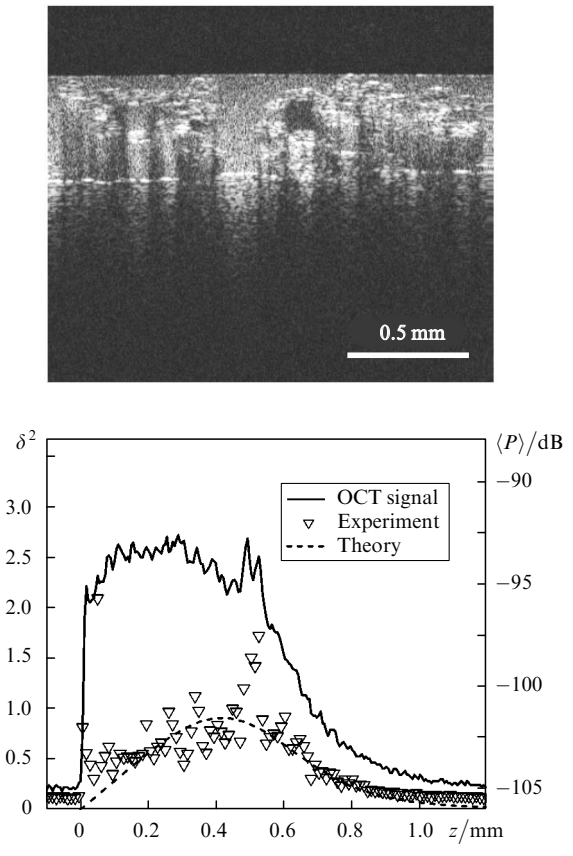


**Figure 7.** OCT image of scattering phantom with random absorption (top) and the results of its statistical analysis (bottom). Solid curve: average OCT signal versus the imaging depth; symbols: the variance of the measured OCT signal relative fluctuations; dashed curve: the analytically calculated variance of OCT signal relative fluctuations. Reconstructed average scattering parameters: $\mu_{fs} = 2.5$ mm$^{-1}$, $\langle\theta^2\rangle = 0.008$. Estimated statistical characteristics of absorption inhomogeneities: $a = 0.04$ mm and $A_0 = 0.31$ mm$^{-1}$.

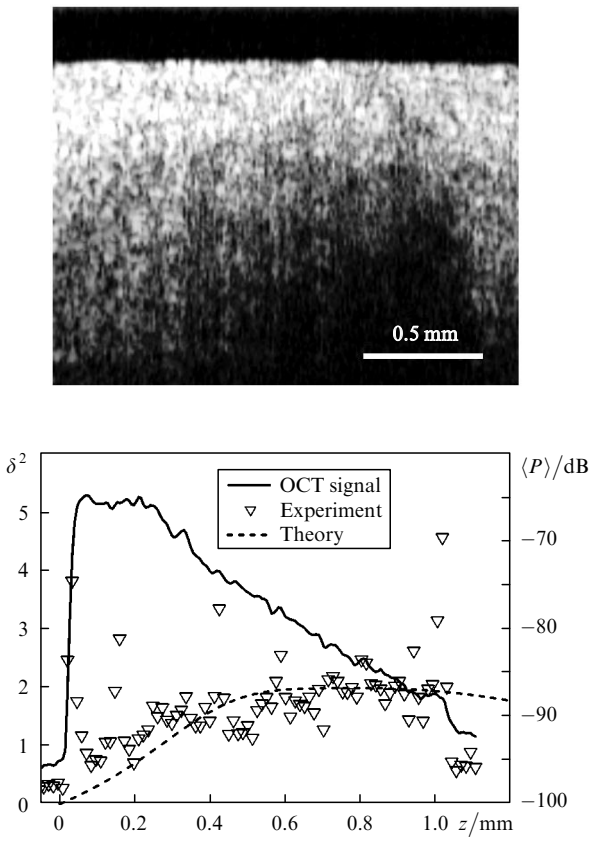


**Figure 8.** OCT image of mucous biotissue (top) and the result of its statistical processing (bottom). Solid curve: average OCT signal versus the imaging depth; symbols: the variance of the measured OCT signal relative fluctuations; dashed curve: the analytically calculated variance of OCT signal relative fluctuations. Reconstructed average scattering parameters: $\mu_{fs} = 6$ mm$^{-1}$, $\langle\theta^2\rangle = 0.08$. Estimated statistical characteristics of absorption inhomogeneities: $a = 0.45$ mm and $A_0 = 0.6$ mm$^{-1}$.

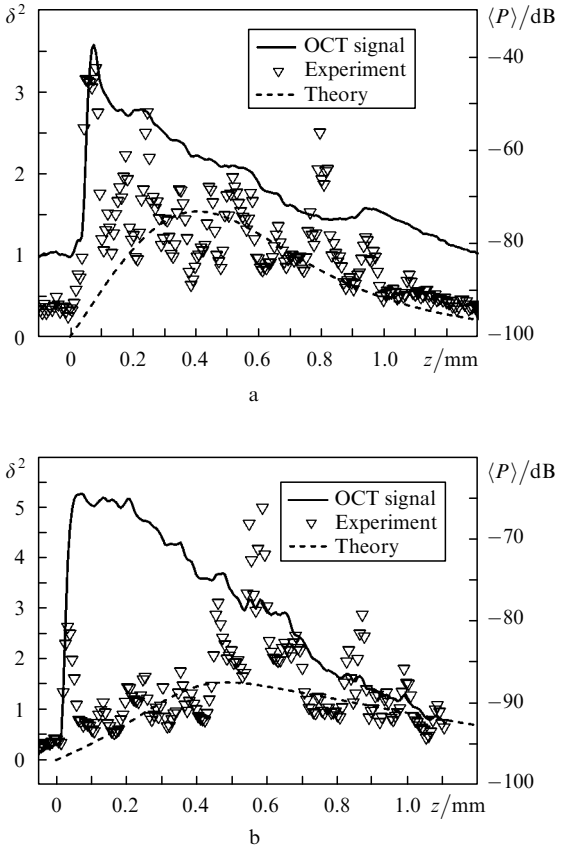


**Figure 9.** Same as in Fig. 8 for different samples of mucous biological tissue: (a) $\mu_{fs} = 14\ \text{mm}^{-1}$, $\langle\theta^2\rangle = 0.04$, $a = 0.2$ mm, $A_0 = 0.9\ \text{mm}^{-1}$; (b) $\mu_{fs} = 6\ \text{mm}^{-1}$, $\langle\theta^2\rangle = 0.08$, $a = 0.3$ mm, $A_0 = 0.55\ \text{mm}^{-1}$.

Figures 8 and 9 show two OCT images of the mucous biological tissue and their statistical processing. The images reveal the presence of shadow noise by the way the OCT signal fluctuates. Though the in-depth dependence of the variance of OCT signal fluctuations from the biotissue is irregular, its average shape is in good agreement with the theoretical curve.

## 4. Discussion

Multiplicative noise is one of the most essential interfering factors which influence the operation of communication, radar and sonar systems etc. Fluctuations of the OCT signal which we called 'shadow noise' demonstrate all features of multiplicative noise: first, they appear due to the random modulation of the signal by statistical inhomogeneities of the medium; second, they limit the accuracy of reflectivity measurements and at the same time they contain useful information about statistical properties of fluctuating optical parameters.

Shadow noise can be distinguished from speckle noise or instrumental noise by its specific properties. This type of noise appears at relatively high levels of the detected signal, the variance of shadow noise depends on the properties of the observed object and is a nonmonotonic function with the regions of rise and fall. Shadow noise is insensitive to the magnitude of the axial resolution which is defined by the probing radiation bandwidth. At the same time, the variance of shadow noise is in direct relation with the transverse resolution of the imaging system since the increase in the probing beam width results in a decrease in both the shadow noise variance and the depth of the maximum noise intensity. Characteristics of shadow noise depend on the average scattering coefficient of the medium; therefore, they are sensitive to the choice of the probing wavelength. The OCT device with the working wavelength within the range of the maximum transparency of the medium provides optimal conditions for detection of shadow noise.

The imaging quality of spatially distributed backscattering structures using OCT in the presence of shadow noise depends on the relationship between the inhomogeneity contrast $k = \tilde{\mu}_{bs}/\langle\mu_{bs}\rangle$ and the variance of OCT signal relative fluctuations $\delta$. As a rough estimate of acceptable visibility one can use the condition $k > \delta$ . In medical OCT devices employed in the performed experiments the maximum variance of OCT signal reaches the values of $\sim 1.5$, which dramatically limits the possibility of observation of 3D structures at the depths where shadow noise is considerable. At the same time, shadow noise does not affect the ability of OCT imaging stratified structures in biotissues.

Absorbing inhomogeneities of a turbid medium appear as dark regions in OCT images; therefore, shadow structures in an image provide information about the distribution of absorbers. However, dark spots in OCT images can also be produced by structures with weak backscattering. Therefore, the demonstrated procedure of reconstructing the statistical parameters of the absorption distribution ($A_0$ and $a$) cannot be applied alone to identify allocation of absorbers in the medium. To solve this problem a method of distinguishing shadow structures in OCT images produced by scattering inhomogeneities from those produced by absorbing ones should be developed. Theoretically this task can be solved based on the fact that an absorbing inclusion provides an extensive underneath shade in an image while back-reflection from a scattering inhomogeneity is exactly related to its location.

## 5. Conclusions

In this paper a theoretical model of OCT images of a turbid medium with a statistically inhomogeneous distribution of optical parameters is proposed. It is assumed that fluctuations of scattering and absorption produce spatial noise in OCT images, which is the result of random extinction of light upon its back and forth passage through the medium. Two basic models of shadow noise are developed which allow one to evaluate the spatial correlation function of OCT signal relative fluctuations. The first model is based on the assumption that the OCT signal is mainly formed by ballistic photons. The second model considers contribution of multiply scattered photons to the detected signal. It is demonstrated that for reflection-mode imaging additional clearing of the medium (the enhanced 'sieve effect') and additional increase in OCT signal fluctuations can be observed due to propagation of light through the same absorbing inhomogeneities upon its back and forth passage in the medium. A hybrid model of shadow noise which accounts for contribution of both ballistic and scattered photons to the OCT signal is developed by combining the two basic models.

Statistical analysis of OCT images of a biological tissue is performed to reveal the presence of shadow noise and to estimate statistical characteristics of this noise. Shadow noise is discovered in the observed images and appears

in OCT signal fluctuations. The experimental dependence of the variance of OCT signal relative fluctuations on the imaging depth has been compared to the theoretical one. Average optical properties of the observed media were estimated from OCT images using the image processing algorithm. Using real OCT images the feasibility to estimate statistical parameters of absorption distribution from shadow noise characteristics is demonstrated.

***Acknowledgements.*** This work was partially supported by the Russian Foundation for Basic Research (Grant No. 07-02-01179), Russian Federal Agency for Science and Innovations (Grant No. 02.522.11.2002), and Presidential Grant for governmental support of Russian leading scientific schools (Grant No. NSh-1244.2008.2).

## References

1. Huang D., Swanson E.A., Lin C.P., Schuman J.S., Stinson W.G., Chang W., Hee M.R., Flotte T., Gregory K., Puliafino C.A., Fujimoto J.G. *Science*, **254**, 1178 (1991).
2. Bouma B.E., Tearney G.J. *Handbook of Optical Coherence Tomography* (New York: Marcel Dekker, 2002).
3. Tuchin V.V. (Ed.) *Handbook of Coherent Domain Optical Methods. Biomedical Diagnostics, Environmental and Material Science* (Boston – Dordrecht – London: Kluwer Acad. Publ., 2004) Vol. 2.
4. Schmitt J.M., Xiang S.H., Yung K.M. *J. Biomed. Opt.*, **4**, 95 (1999).
5. Kholodnykh A.I., Petrova I.Y., Larin K.V., Motamedi M., Esenaliev R.O. *Appl. Opt.*, **42**, 3027 (2003).
6. Mullamaa Yu.R. (Ed.) *Stochastic Structure of Cloud and Radiation Fields* (Washington: NASA Technical Translation F-822, 1975).
7. Borovoi A.G. *Dokl. Akad. Nauk SSSR*, **276**, 1374 (1984).
8. Dolin L.S. *Dokl. Akad. Nauk SSSR*, **277**, 77 (1984).
9. Fukshansky L. *J. Quant. Spectr. Rad. Transfer*, **38**, 389 (1987).
10. McClendon J.H., Fukshansky L. *J. Photochem. Photobiol.*, **51**, 211 (1990).
11. Kliorin N.I., Kravtsov Yu.A., Mereminskii A.E., Mirovskii V.G. *Radiophysics and Quantum Electronics*, **32**, 793 (1989).
12. Anisimov O., Fukshansky L. *J. Quant. Spectr. Rad. Transfer*, **48**, 169 (1992).
13. Dolin L.S. *Radiophysics and Quantum Electronics*, **49**, 719 (2006).
14. Dolin L.S., Shchegolkov Yu.B., Shchegolkov D.Yu. *Radiophysics and Quantum Electronics*, **51** (3), 222 (2008).
15. Dolin L.S. in *Oceanic and Atmospheric Optics: Proc. of Fourth Workshop on Ocean Optics* (Baku: ELM, 1983) p. 147.
16. Zege E.P., Ivanov A.P., Katsev I.L. *Image Transfer Through a Scattering Medium* (Heidelberg: Springer-Verlag, 1991).
17. Dolin, L.S., Saveliev V.A. *Izv. Akad. Nauk SSSR: Fiz. Atmos. Okean.*, **36**, 794 (2000).
18. Dolin L.S., Levin I.M. *Spravochnik po teorii podvodnogo videniya* (Handbook on Underwater Imaging Theory) (Leningrad: Gidrometeoizdat, 1991).
19. Rytov S.M., Kravtsov Y.A., Tatarski V.I. *Principles of Statistical Radiophysics* (Berlin: Springer, 1987) Vol. 2.
20. Kravtsov Yu.A., Saichev A.I. *Sov. Phys. Uspekhi*, **25**, 494 (1982).
21. Turchin I.V., Sergeeva E.A., Dolin L.S., Kamensky V.A., Shakhova N.M., Richards-Kortum R. *J. Biomed. Opt.*, **10**, 064024 (2005).